
Article:
Petrenas, R., Hawkins, O.A., Jones, J.F. orcid.org/0009-0004-6876-9243 et al. (8 more authors) (2025) Confinement and catalysis within de novo designed peptide barrels. Journal of the American Chemical Society, 147 (4). pp. 3796-3803. ISSN 0002-7863

https://doi.org/10.1021/jacs.4c16633

JACS
JOURNAL OF THE AMERICAN CHEMICAL SOCIETY
pubs.acs.org/JACS

Article

Confinement and Catalysis within *De Novo* Designed Peptide Barrels

Rokas Petrenas, Olivia A. Hawkins, Jacob F. Jones, D. Arne Scott, Jordan M. Fletcher, Ulrike Obst, Lucia Lombardi, Fabio Pirro, Graham J. Leggett, Thomas A.A. Oliver,* and Derek N. Woolfson*

Cite This: *J. Am. Chem. Soc.* 2025, 147, 3796−3803

Read Online

ACCESS | Metrics & More | Article Recommendations | Supporting Information

ABSTRACT: *De novo* protein design has advanced such that many peptide assemblies and protein structures can be generated predictably and quickly. The drive now is to bring functions to these structures, for example, small-molecule binding and catalysis. The formidable challenge of binding and orienting multiple small molecules to direct chemistry is particularly important for paving the way to new functionalities. To address this, here we describe the design, characterization, and application of small-molecule:-peptide ternary complexes in aqueous solution. This uses α-helical barrel (αHB) peptide assemblies, which comprise 5 or more α helices arranged around central channels. These channels are solvent accessible, and their internal dimensions and chemistries can be altered predictably. Thus, αHBs are analogous to "molecular flasks" made in supramolecular, polymer, and materials chemistry. Using Förster resonance energy transfer as a readout, we demonstrate that specific αHBs can accept two different organic dyes, 1,6-diphenyl-1,3,5-hexatriene and Nile red, in close proximity. In addition, two anthracene molecules can be accommodated within an αHB to promote anthracene photodimerization. However, not all ternary complexes are productive, either in energy transfer or photodimerization, illustrating the control that can be exerted by judicious choice and design of the αHB.

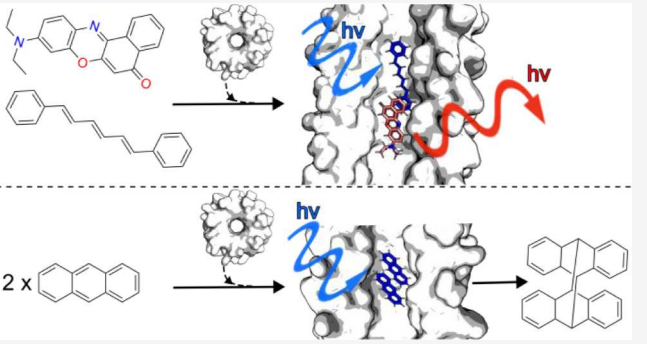

1. INTRODUCTION

Natural enzymes catalyze chemical reactions with high substrate specificity, product stereoselectivity, and substantial accelerations of reaction rates. Designable and tunable enzyme-like catalysts would have wide-ranging applications in basic science, chemical synthesis, and the biotech and pharmaceutical industries. Despite considerable advances in the past four decades,[1−6] truly *de novo* peptide and protein design for small-molecule binding and efficient catalysis remains a significant challenge.[7−9]

Early *de novo* structural design used straightforward patterning of hydrophobic and polar residues to deliver peptide assemblies that mimicked simple protein architectures.[1,3] Some of these have been embellished with metal-binding sites leading to catalysis.[3,10,11] These minimal approaches gave way to rational design, in which sequence design was augmented by sequence-to-structure/function relationships garnered from natural proteins to produce a wider variety of robust peptide and protein designs.[1,12] Such designs have also been functionalized to yield hydrolases and various metalloenzymes among other activities.[11,13−17] In parallel with these developments, computational protein design has emerged to deliver methods for backbone constructions, for fitting *de novo* sequences onto these scaffolds, and for assessing the quality of the models ahead of experiments.[11,18] Early computational protein design also introduced modeling of protein−ligand interactions.[19] This led to natural protein scaffolds being repurposed for binding and catalysis.[20−22] Currently, the field is undergoing another step-change with the application of deep-learning methods to generate *de novo* protein sequences, structures, and functions.[5,23−25] This has allowed the design of complex structures with tailored binding functions, in some cases with nanomolar affinity and sub-Å accuracy.[7,8,26] However, overall success rates of completely *de novo* small-molecule binders and enzymes remain low and usually require screening of large libraries and/or further optimization *via* directed evolution.[6−9]

Despite this trajectory and advances in rational and computational design, there are very few successful examples of bringing two or more ligands together into a fully *de novo* designed protein binding site.[27,28] However, with many cofactor-like catalysts available,[29] reactions in aqueous solutions could be accelerated by confining and orienting multiple small molecules within minimal binding sites to direct chemistry between them.

Received: November 22, 2024
Revised: December 27, 2024
Accepted: December 30, 2024
Published: January 15, 2025

Although catalysis by confinement is observed in natural enzymes,[30] the concept of "molecular flasks" has been exploited broadly in supramolecular and polymer chemistry, where reactions in aqueous solution are accelerated by encapsulating guest molecules in micelles,[31] organometallic cages[32,33] or ordering of molecules by crystallization.[34,35] Perhaps the most biomimetic are the organometallic cages, as the shape and size of a hydrophobic pocket controls ligand binding and regio- and stereoselectivity of a reaction, including new reactions not possible in free solution.[32,33] Examples of reactions catalyzed by these cages include regioselective 1,3-dipolar cycloadditions, and a novel Diels–Alder reactivity between inert arenes and N-substituted maleimides.[32]

Over the past decade, a range of oligomeric α-helical barrels (αHBs) has been designed based on self-assembling peptides.[36−38] Similarly to molecular flasks,[39] these αHB assemblies have solvent-accessible lumens that can bind small molecules, including reporter fluorescent dyes such as 1,6-diphenyl-1,3,5-hexatriene (DPH) and 1-[6-(dimethylamino)-2-naphthalenyl]-1-propanone (prodan).[37,40] The αHBs present interesting *de novo* scaffolds because of their stability, controllable oligomeric states and lumen sizes, robustness to mutation, and the potential to functionalize the internal channels for small-molecule binding and catalysis by incorporating both proteinogenic and noncanonical amino acids.[13,41]

Inspired by the simplicity of molecular flasks, here we explore if αHBs can controllably bind two different small molecules and orient them for catalysis. By combining ultrafast spectroscopic methods to monitor Förster resonance energy transfer (FRET) and molecular dynamics simulations, we demonstrate that specific αHBs can accommodate two different organic dyes, DPH and Nile red in close proximity. In addition, two anthracene molecules can be bound within the αHBs to promote or inhibit anthracene-dimer formation.

2. RESULTS AND DISCUSSION

2.1. αHBs Can Encapsulate Pairs of Small Molecules.

The lengths and widths of the channel in hexameric and heptameric αHBs (~46 × 7 Å and ~46 × 8 Å, respectively) are larger than ligands such as DPH (~14 × 4 Å).[37] Therefore, we hypothesized that it should be possible to bind multiple copies of such ligands within a single channel simultaneously, and potentially in conformations leading to productive interactions. We chose to probe possible ternary complex formation through FRET. DPH was chosen as a potential FRET donor as it binds to multiple αHBs with μM affinities, characterized by a large increase in DPH fluorescence intensity.[41] However, none of the dye molecules studied to date that bind αHBs have appreciable overlapping absorption with DPH emission and, thus, are not suitable as FRET acceptors.[37,41] We identified three potential DPH-FRET acceptors with favorable characteristics for αHB binding: Methyl orange, Coumarin-7 and Nile red.[42]

Modeling with AutoDock Vina[43] predicted strong binding for Coumarin-7 (−9.0 kcal mol^{-1}) and Nile red (−9.2 kcal mol^{-1}) with the heptameric αHB (CC-Type2-[I_aV_d], PDB code 6g66). Although it still docked within the hydrophobic channel, Methyl orange was predicted to bind the αHB more weakly (−6.7 kcal mol^{-1}, Figures S3 and S4). Consistent with these predictions, experimentally, both Coumarin-7 and Nile red bound the heptameric αHB with μM affinities and showed signatures of FRET with donor DPH (Figures 1 and S5).

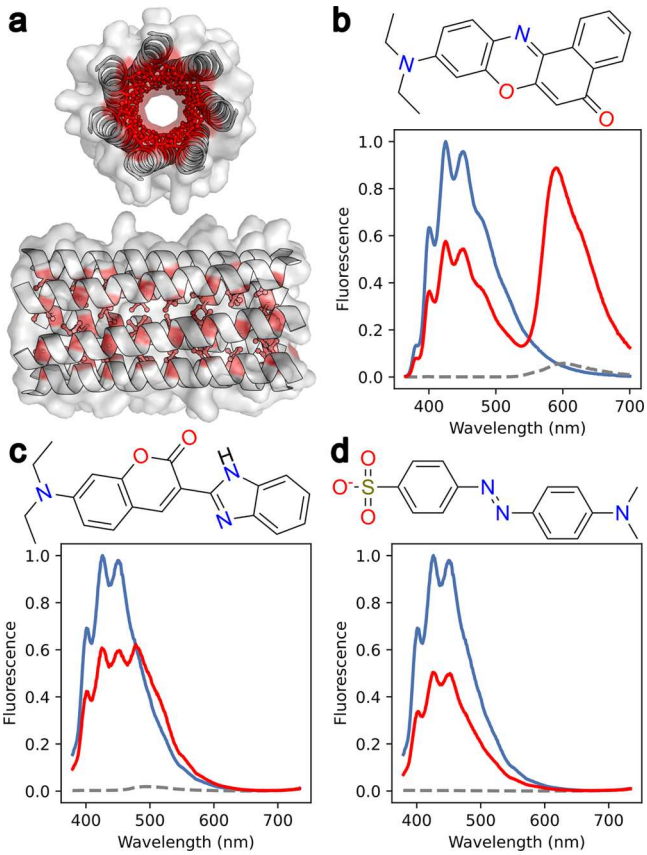

Figure 1. Nile red and Coumarin-7 are FRET acceptors with DPH donor in the presence of an αHB. (a) Surface and cartoon representation of the heptameric αHB crystal structure (PDB code 6g66). The hydrophobic channel is depicted by red sticks. (b–d) Steady-state emission spectra after DPH excitation within the heptamer with (b) Nile red, (c) Coumarin-7, and (d) Methyl orange. Conditions: λ_{ex} = 352 nm, 3 μM potential acceptor 3 μM DPH, 5 μM peptide assembly, HEPES, 10% v/v MeCN, pH 7. Key: DPH emission spectrum, blue line; acceptor emission spectrum, broken black line; mixed DPH + acceptor emission spectrum, red line.

Conversely, Methyl orange did not bind or show any FRET signal. Nile red was selected as a FRET acceptor for further study as its emission was the most intense and its fluorescence maxima significantly red-shifted from the peak of DPH's emission (Figure 1).

With this potential FRET pair in hand, we screened a wider set of αHBs for Nile red binding and FRET efficiency. We restricted the screen to 15 open αHBs with hexameric to octameric oligomeric states and luminal hydrophobic aliphatic and/or aromatic residues (Table S1).[41] As a negative control, we included a 3-helix bundle without a channel (PDB code 4dzl).[37] This screen confirmed Nile red binding to all 15 αHBs through steady-state emission spectra. Like DPH, the Nile red fluorescence intensity was significantly increased when incubated with the αHBs as compared to the control (see Figures S6 and S7).

The screen identified 10 peptides that showed FRET between DPH and Nile red (Figures 2a and S8). We were unable to rationalize the different FRET efficiencies from peptide sequences alone. However, αHBs with the highest FRET efficiencies could be identified from predicted ternary-complex energies and distances from docking simulations (Figure S9).

https://doi.org/10.1021/jacs.4c16633
J. Am. Chem. Soc. 2025, 147, 3796−3803

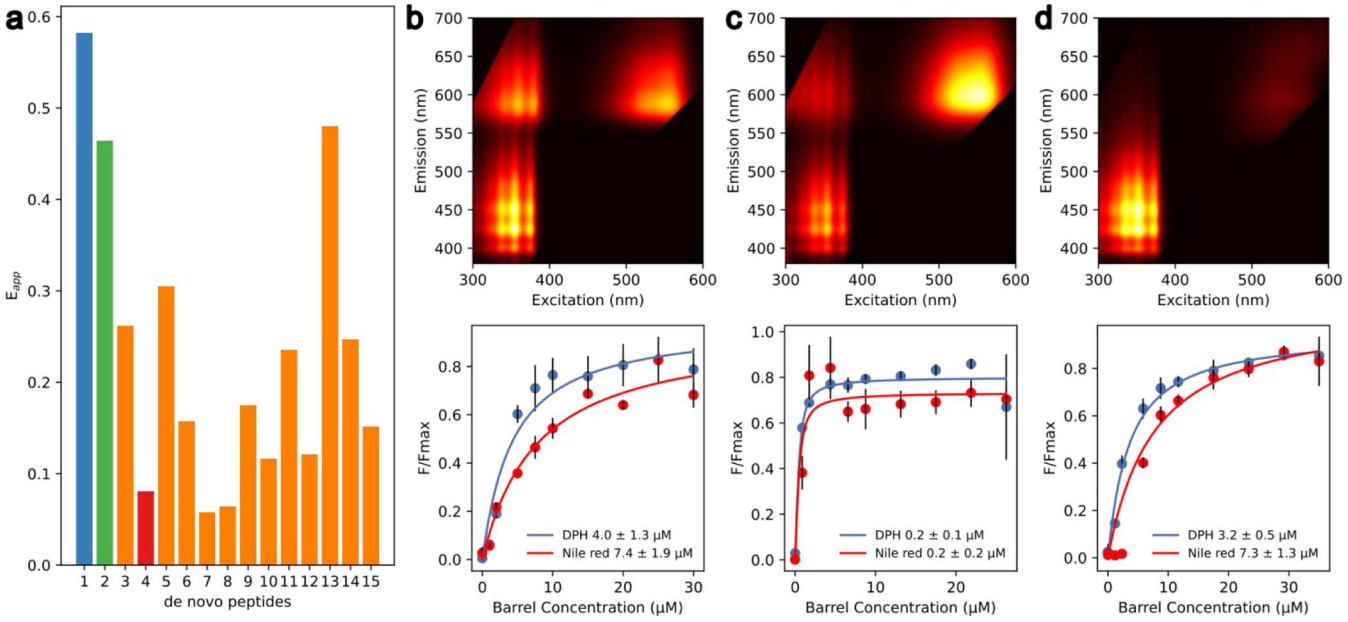

Figure 2. Screening for αHBs that coencapsulate DPH and Nile red. (a) Apparent steady-state FRET efficiency for the 15 screened peptides with the heptamer in blue (#1); the octamer, green (#2); the hexamer, red (#4); and the remaining peptides, orange. $E_{app} = \frac{I(acceptor)}{I(acceptor) + I(donor)}$. 2D excitation−emission spectra and the saturation binding curves for the top two hits: (b) the heptamer, (c) the octamer, and (d) a negative hit, the hexamer. F/F_{max}: normalized fluorescence at 450 nm (DPH, blue) or 593 nm (Nile red, red). Fluorescence conditions: 3 μM Nile red, 3 μM DPH, 5 μM peptide assembly. Saturation binding curve conditions: 0.5 μM DPH or Nile red, 0−30 μM peptide assembly, data are the mean of three independent repeats, and error bars represent the standard deviation from the mean. All data collected in HEPES, 10% v/v MeCN, pH 7. See Table S1 for peptide biophysical data and sequences. See Figure S8 for the steady-state FRET spectra.

We selected the two αHBs that generated strong steady-state FRET signals for further characterization: heptameric CC-Type2-[I_aV_d] and octameric CC-Type2-[I_aI_d]−I17 V-I21F (PDB codes 6g66 and 9f5a). Strong steady-state FRET was also observed with peptide #13 (Figures 2a and S8, Table S1), but this was not investigated further as we were unable to crystallize this peptide and fully confirm its structure. Both selected barrels bound DPH and Nile red with low μM affinities, and we did not observe strong cooperativity or competition between the ligands (Figure S10). 2D excitation−emission data showed that FRET occurred from all vibronic states of the lowest energy DPH absorption band (Figure 2b,c), as evident from the strong "cross-peaks" in the upper left quadrants of the correlation maps.

As a control for experiments described below, we chose a hexameric αHB (CC-Type2-[$S_gL_aI_d$]; PDB code 4pn9), which showed strong emission from DPH and Nile red individually but did not exhibit FRET (Figures S6−S8). Despite μM affinities for both ligands (Figure 2d), DPH could displace Nile red from this αHB, as evident from a strong decrease in Nile red fluorescence intensity (Figure S12). This barrel illustrates how cavity shape and size alone can lead to specificity between two ligands with similar physical and chemical properties.

Finally, we used analytical ultracentrifugation to confirm that the oligomeric states of the barrels with bound ligand matched those observed by crystallography (Figure S13). For simplicity, henceforth we refer to the three αHB peptides CC-Type2-[$S_gL_aI_d$], CC-Type2-[I_aV_d] and CC-Type2-[I_aI_d]−I17V-I21F, as the hexamer, heptamer and octamer, respectively.

2.2. αHBs Increase Energy Transfer Rate between DPH and Nile Red. To characterize the interaction between DPH and Nile red in αHBs further, we measured the time scales of energy transfer between the donor (DPH) and acceptor (Nile red) dyes as these are highly sensitive to the intermolecular separation distance. This used time-correlated single-photon counting (TCSPC) and transient absorption (TA) spectroscopy performed on ternary complexes with the heptamer and the octamer αHBs.

First, we measured the fluorescence lifetimes for each dye individually in the barrels. Direct excitation of DPH at 352 nm yielded average fluorescence lifetimes of 15.9 ± 0.2 ns with the heptamer, and 15.8 ± 0.2 ns with the octamer (Table S5 and Figure S17). For Nile red, the corresponding control measurements used 535 nm light to selectively excite the dye. This yielded fluorescence lifetimes of 4.10 ± 0.2 ns (with the heptamer) and 4.2 ± 0.2 ns (octamer) (Table S6 and Figure S19). In the presence of DPH, these increased to 4.9 ± 0.2 ns and 5.1 ± 0.2 ns, respectively (Table S7 and Figure S19). This increase in Nile red's fluorescence lifetime and small changes in the steady-state spectra (Figure S14) suggest that DPH alters the binding environment of Nile red in the αHBs.

Consistent with the hexamer providing a more hydrophobic environment due to its smaller channel radius, control measurements of each dye showed even longer fluorescence lifetimes: 4.9 ± 0.17 ns for Nile red and 19.8 ± 0.17 ns for DPH (Tables S5 and S6). Overall, when bound to the αHBs, the fluorescence lifetimes of DPH and Nile red are at least as long as those previously reported in nonpolar solvents, indicative of binding within enclosed hydrophobic environment.[44−47]

Next, we measured the time scale for energy transfer between DPH and Nile red after direct and *selective* photoexcitation of DPH at 352 nm. Analysis of these data yielded FRET time constants of 0.98 ± 0.2 ns for the heptamer and 1.3 ± 0.2 ns for the octamer (Figures 3a and S22). Using

https://doi.org/10.1021/jacs.4c16633
J. Am. Chem. Soc. 2025, 147, 3796−3803

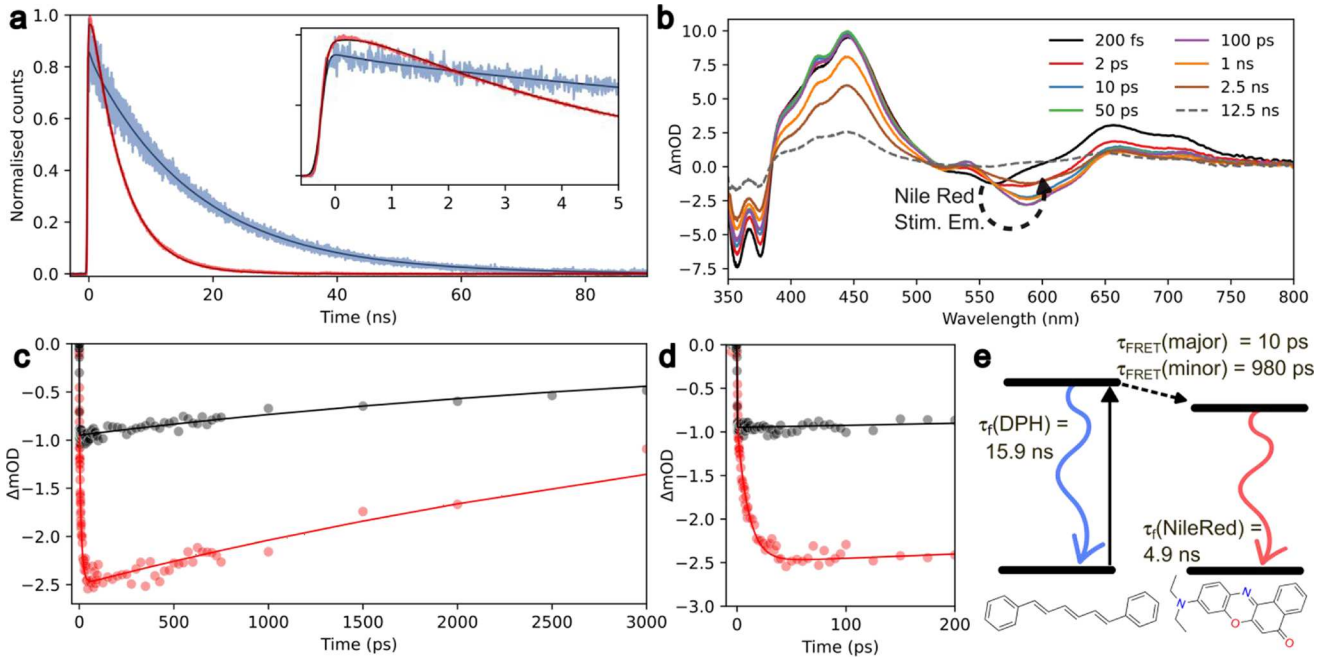

Figure 3. TCSPC and transient absorption measurements reveal ultrafast FRET between DPH and Nile red. (a) Fluorescence decay in the heptamer for DPH (blue) and Nile red (red) after excitation at 352 nm. (b) Wavelength resolved transient absorption of the heptamer for DPH and Nile red after 352 nm excitation for 8 different pump−probe time delays. ΔmOD: change in milli-optical density. (c) Kinetics obtained by integration over the Nile red stimulated emission signal for the heptamer with Nile red after 535 nm excitation (black circles) and the heptamer with DPH and Nile red using 352 nm photoexcitation (red circles), and overlaid fits (solid lines). (d) Early time dynamics of the data shown in (c) illustrating the difference between photoexcitation of DPH or Nile red on the Nile red stimulation emission kinetics. (e) Kinetic model of FRET and radiative decay pathways determined for DPH and Nile red in the heptamer. Similar time constants were obtained for the octamer (Tables S5−S9). TCSPC conditions: 3 μM DPH and Nile red, 5 μM peptide assembly, HEPES, 10% v/v MeCN, pH 7. TA conditions: 10 μM DPH and Nile red, 15 μM peptide assembly, HEPES, 10% v/v MeCN, pH 7. For TCSPC fitting parameters and time-resolved emission spectra, see Tables S5−S8, Figures S22 and S23. For TA fitting parameters and wavelength resolved transient absorption, see Table S9 and Figure S26.

the Förster equation (eq S6), the internuclear distance between DPH and Nile red was estimated as 3.3−3.9 nm for the heptamer, and 3.1−3.9 nm for the octamer (Figures S24 and S25). These are well within the length of the hydrophobic channels at ∼4.6 nm and demonstrate successful encapsulation of both DPH and Nile red within the same barrel. As anticipated from steady-state fluorescence experiments (Figure 2d), no evidence for FRET was observed in the hexamer from TCSPC measurements (Figures S17−S21 and Tables S5−S7).

The relative amplitude of the fluorescence rise component in the TCSPC measurements was surprisingly small despite sizable cross-peaks in 2D fluorescence maps and negligible direct excitation of Nile red (Figures 2 and S8). This implies that most Nile red molecules undergo energy transfer on time scales faster than the instrument response function (IRF) for the TCSPC experiment (170 ps).

To probe the possibility of faster FRET dynamics in αHBs, transient absorption (TA) spectroscopy with 3 orders of magnitude higher time resolution (IRF ∼ 280 fs), was applied to the complexes with heptameric and octameric barrels (Figure 3b−d). Spectral assignments of the main features of the TA data are given in Figure S26. Critically, a negative signal centered at 590 nm rose within the first few picoseconds associated with stimulated emission from Nile red with both the heptamer and octamer (see kinetics in Figure 3c,d). The delayed rise originates from prompt energy transfer between DPH and Nile red, and subsequent fluorescence from Nile red. In contrast, control measurements that directly excited Nile red (Figure S26) showed this band immediately (Figure 3c,d) confirming the delayed rise must be from energy transfer. Analysis of the data returned fast energy transfer time constants between DPH and Nile red: 10.4 ± 2.4 ps (Figure 3c and Table S9) in the heptamer, and 7.9 ± 5.7 ps (Figure S28 and Table S9) in the octamer, reconciling the high energy transfer efficiency determined from steady state emission measurements. A secondary ∼1 ns rise in the stimulated emission signal was not evident within the TA data, as would be expected from TCSPC measurements. We suggest that this is because the ∼1 ns FRET component corresponds to a minority population, which is only observed in TCSPC measurements due to the technique's sensitivity to only fluorescence and higher signal-to-noise ratios.

We rationalize these different observations by the presence of two conformationally different states present in both of the investigated αHBs: 1) a dominant population where DPH and Nile red are in close proximity facilitating rapid energy transfer on a ∼10 ps time scale; and 2) a minor population where DPH and Nile red are located ∼3 nm apart within a barrel and undergo a slower energy transfer with a time constant of ∼1 ns (Figure 3e).

2.3. Molecular Dynamics Simulations Indicate Favorable Stacking between Dyes. To investigate the two states proposed from ultrafast spectroscopy measurements further, we used docking and molecular dynamics (MD) simulations to explore the DPH and Nile red binding conformations within the αHBs. Three 0.5 μs MD simulations of a DPH:Nile red:heptamer complex were initiated from three distinct poses. The latter were generated by simultaneously docking DPH and Nile red into the αHB crystal structures using AutoDock Vina (Figure S29).[43] The MD simulations indicated that the

https://doi.org/10.1021/jacs.4c16633
J. Am. Chem. Soc. 2025, 147, 3796−3803

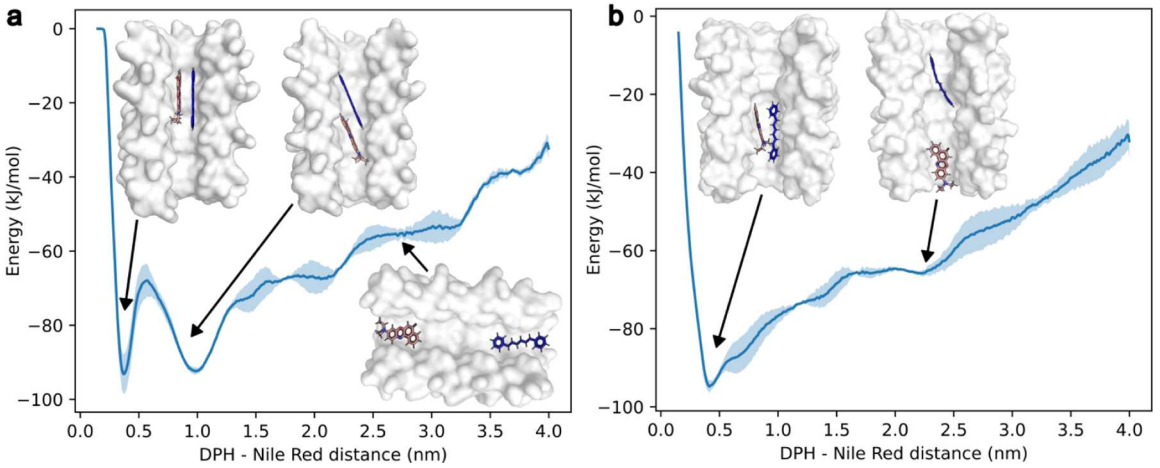

Figure 4. Free energy landscape sampling the distance between DPH (blue) and Nile red (red) within the αHBs. (a) The heptamer has two minima at 3.5 Å (-93 ± 5 kJ mol^{-1}) and 10.0 Å (-92 ± 1 kJ mol^{-1}). (b) The octamer shows a broad global minimum at 4.1 Å (-94.6 ± 2 kJ mol^{-1}). 3 ×1 μs simulations were started independently from the starting poses in Figures S29 and S35. Standard deviation from the mean is shown in pale blue.

complexes were stable, with DPH and Nile red remaining either fully π-stacked within 3.5 Å or slipped-stacked within 10.0 Å distances (measured from their centers of mass) throughout simulations in the heptamer (Figure S30). The overall αHB conformation did not change significantly from the determined X-ray crystal structure through the trajectories, with the majority of C_α backbone root-mean-square fluctuation $\leq$0.5 Å (Figures S31−S34). Similar results were obtained for the octamer αHB (Figures S35−S40).

Since the ligand movement along the channel (z) axis was slow (Figures S33 and S39), metadynamics simulations were initiated for the three docking poses within the heptamer to ensure that local minima of the energy landscape were explored. The distance between DPH and Nile red was used as a bias variable and sampled from 1.5 to 40 Å to observe many conformations along the entire channel. After 1 μs, all three simulations converged to the same free-energy surface irrespective of the starting position of the simulation (Figure 4a). The free-energy surface had 2 deep minima with 3.5 and 10.0 Å separations, corresponding to the distances observed with docking and traditional MD simulations (Figures 4a and S29). Shallower local minima were also observed between 20−30 Å. For the octamer, we observed a broad global minimum at 4.1 Å and a shallower minimum around 20 Å (Figure 4b). The closer internuclear distance between DPH and Nile red matched well with the ∼10 ps ultrafast energy transfer time constant between the dyes observed in TA spectroscopy. The shallower higher energy minima at greater dye separations will have a lower population at room temperature, and thus represent a small percentage of the total sample, which possibly correspond to the conformations that undergo slower ∼1 ns dynamics, as extracted from TCSPC measurements.

2.4. αHBs Encapsulate Anthracene and Promote Its Photodimerization. Encouraged by the successful demonstration of energy transfer between DPH and Nile red with clear co-occupancy of the dyes in the heptameric and octameric barrels, and the modeling indicating intermolecular π-stacking (Figure 4), we investigated if similar interactions could be promoted and exploited in αHBs for different hydrophobic molecules. Anthracene was chosen as, when preorganized into a π-stacked dimer, it undergoes a well-characterized [4 + 4] cycloaddition reaction upon UV-irradiation at 365 nm. This is readily followed spectroscopically even at μM concentrations, as photodimerization reduces anthracene emission.

In silico docking of two anthracene molecules with the heptamer predicted two poses: a potentially reactive π-stacked dimer with a 3.5 Å separation, and a slip-stacked conformation (Figure 5a). Starting from these poses, 0.5 μs MD simulations revealed the ternary complex to be highly dynamic, with

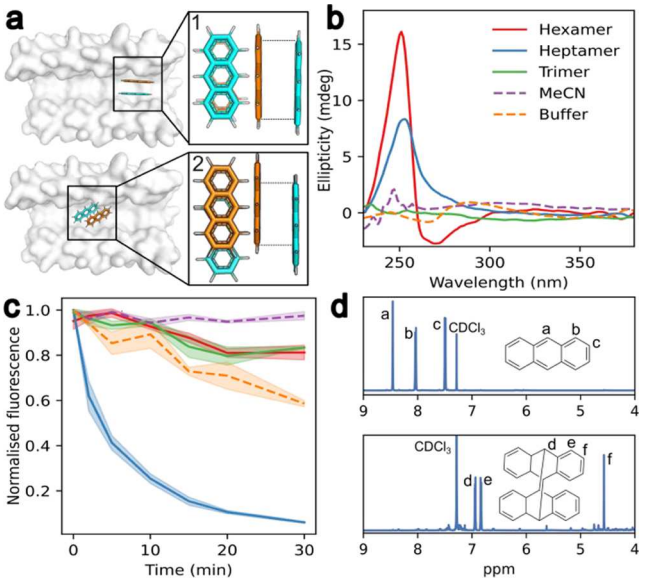

Figure 5. αHB channel dimensions control anthracene photodimerization in aqueous solution. (a) Lowest energy AutoDock Vina poses (both -18.7 kcal mol^{-1} dimer) for anthracene dimer in the heptamer, showing reactive (1) and offset (2) conformations. (b) Induced CD signal upon anthracene binding to the heptamer and the hexamer. (c) Decrease in anthracene emission upon irradiation at 365 nm. Color key same as in (b): hexamer, red; heptamer, blue; trimer, green; MeCN, purple; buffer, orange. (d) Proton NMR spectra without illumination (top) and after 30 min of excitation at 365 nm (bottom) for anthracene dimerization reaction within the heptamer. Conditions: 14 μM anthracene, 7 μM peptide assembly, HEPES, 10% v/v MeCN, pH 7, and peptides were removed before collecting NMR data.

https://doi.org/10.1021/jacs.4c16633
J. Am. Chem. Soc. 2025, 147, 3796−3803

anthracene molecules in an equilibrium between a monomer and a π-stacked dimer (Figure S41). By contrast, docking with the hexamer indicated that its diameter would be insufficient to accommodate two fully π-stacked anthracene molecules (Figure S42). Both barrels bound anthracene with low μM affinities (Figure S43). Furthermore, we confirmed anthracene encapsulation experimentally through cosedimentation during ultracentrifugation (Figure S45), and by observing an induced circular dichroism (CD) signal (Figure 5b). The latter is a consequence of the Cotton effect, and only evident when anthracene molecules are encapsulated in a chiral environment, *i.e.* like the lumen of an αHB.[48] As before, we used the trimeric peptide as a control. For the trimer, anthracene cosedimentation was observed, but no induced CD signal was evident, confirming only nonspecific interactions between anthracene and the trimer peptide (Figures S43, S45, and 5b).

Based on modeling and the CD data, we hypothesized that the heptamer could promote anthracene dimerization while the hexamer should inhibit it. When mixed in a 1:2 (αHB:anthracene) ratio and irradiated with 365 nm light, the photodimerization reaction proceeded to completion with the heptamer as indicated by a decrease in fluorescence signal over 30 min (Figure 5c). Complete conversion to the photodimer product was confirmed by ^{1}H NMR (Figure 5d). By contrast, no clear reaction was observed with the hexamer (Figure 5c) other than a much slower, linear loss of anthracene fluorescence similar to the buffer-only, acetonitrile, and trimer controls. These experiments show how encapsulation of the anthracene within the heptamer greatly accelerates photodimerization, presumably by binding two anthracene molecules in a complex primed for [4 + 4] cycloaddition. We also tested the octamer in this reaction, although docking predicted that its channel should be too wide for precise anthracene π-stacking (Figure S46). Consistent with this, while the octamer did promote the conversion, the loss of anthracene fluorescence signal was linear, slower than with the heptamer, and similar to the controls (Figure S47). This highlights that not all αHBs are fully compatible with the transformation, and that selectivity can be achieved by judicious choice of barrel, which is best guided by modeling.

3. CONCLUSIONS

We have demonstrated the ability of the lumens of *de novo* designed α-helical barrel assemblies (αHBs) to bind and organize two ligands in conformations that accelerate the time scales for two different photoinduced chemical processes. First, we show that by exploiting different sizes and shapes of their hydrophobic lumens, we can select αHBs that facilitate energy transfer between two fluorophores, DPH and Nile red. Using ultrafast spectroscopy, we demonstrate that the channels of heptameric and octameric peptide assemblies are long enough to encapsulate both dyes simultaneously, and wide enough to juxtapose them for efficient energy transfer on picosecond time scales. Molecular dynamics simulations predict that DPH and Nile red bind in π-stacked complexes facilitating the observed fast energy transfer. Moreover, by varying the internal diameter of the structures (~7 Å in the hexamer *vs* ~8 Å in the heptamer), we can select for barrels that instead of promoting FRET, preferentially encapsulate only one of the dyes. These two features—ligand encapsulation with (i) selective binding and (ii) in reactive conformations—are the key features of enzymes. Here, we achieve these features through shape complementarity and nonspecific hydrophobic interactions within symmetric peptide assemblies as compared to the more-complex active sites found in natural enzymes. To illustrate the potential of the αHBs in catalysis in aqueous buffers, we have explored the generation of tightly packed anthracene dimers that are primed for a photodimerization reaction. We find that cycloaddition is accelerated within a heptameric αHB, but not within the narrower hexamer. Again, as indicated by predictive modeling, these behaviors appear to be controlled by the relative sizes and shapes of internal lumens of the αHBs.

In the broader context of *de novo* peptide and protein design, current approaches toward developing small-molecule binders and catalysts often rely on deep-learning methods, which do not necessarily enhance our understanding of protein function. In contrast, we control binding and reactivity in a rational and predictive manner by leveraging the concept of "molecular flasks" borrowed from supramolecular chemistry.

Looking ahead, these peptide-based *de novo* designed αHBs are thermostable and tolerate a large number of mutations in their lumens,[41] including to polar, charged, aromatic and noncanonical side chains. As a result, a wide range of small molecules could be encapsulated within the αHBs for manipulation.[41] Moreover, recently, we have shown that the αHB peptide assemblies can be converted to thermostable single-chain proteins by linking multiple helices together through computational protein design.[49] These single-chain proteins are produced by expression from synthetic genes, which opens possibilities for desymmetrization and functionalization through further rational computational protein design, and to improve activity using directed evolution.[6,50] Thus, the αHB peptides and proteins offer an exciting platform for combining the shape complementarity and confinement offered by organic molecular flasks with the diversity of binding-site geometries and substrate selectivity seen in natural enzymes.

■ ASSOCIATED CONTENT

Data Availability Statement

The data underlying this study are openly available in Zenodo at DOI: 10.5281/zenodo.13335904.

Supporting Information

The Supporting Information is available free of charge at https://pubs.acs.org/doi/10.1021/jacs.4c16633.

Experimental materials and methods, peptide sequences, additional steady-state and ultrafast spectroscopy data and fits, and additional docking and molecular-dynamics simulations data (PDF)

■ AUTHOR INFORMATION

Corresponding Authors

Thomas A.A. Oliver − *School of Chemistry, University of Bristol, Bristol BS8 1TS, U.K.;* orcid.org/0000-0003-3979-7857; Email: tom.oliver@bristol.ac.uk

Derek N. Woolfson − *School of Chemistry, University of Bristol, Bristol BS8 1TS, U.K.; Max Planck-Bristol Centre for Minimal Biology and Bristol BioDesign Institute, University of Bristol, Bristol BS8 1TS, U.K.; School of Biochemistry, University of Bristol, Bristol BS8 1TD, U.K.;* orcid.org/0000-0002-0394-3202; Email: d.n.woolfson@bristol.ac.uk

Authors

Rokas Petrenas − *School of Chemistry, University of Bristol, Bristol BS8 1TS, U.K.*

https://doi.org/10.1021/jacs.4c16633
J. Am. Chem. Soc. 2025, 147, 3796−3803

Olivia A. Hawkins − *School of Chemistry, University of Bristol, Bristol BS8 1TS, U.K.*
Jacob F. Jones − *School of Chemistry, University of Bristol, Bristol BS8 1TS, U.K.;* orcid.org/0009-0004-6876-9243
D. Arne Scott − *Rosa Biotech, Science Creates St Philips, Bristol BS2 0XJ, U.K.*
Jordan M. Fletcher − *Rosa Biotech, Science Creates St Philips, Bristol BS2 0XJ, U.K.*
Ulrike Obst − *Rosa Biotech, Science Creates St Philips, Bristol BS2 0XJ, U.K.*
Lucia Lombardi − *School of Chemistry, University of Bristol, Bristol BS8 1TS, U.K.; Department of Chemical Engineering, Imperial College London, London SW7 2AZ, U.K.;* orcid.org/0000-0002-5202-9847
Fabio Pirro − *School of Chemistry, University of Bristol, Bristol BS8 1TS, U.K.*
Graham J. Leggett − *School of Mathematical and Physical Sciences, University of Sheffield, Sheffield S3 7HF, U.K.;* orcid.org/0000-0002-4315-9076

Complete contact information is available at: https://pubs.acs.org/10.1021/jacs.4c16633

Author Contributions

The manuscript was written with contributions from all authors.

Notes

The authors declare no competing financial interest.

■ ACKNOWLEDGMENTS

R.P. is supported by a BBSRC-funded PhD studentship and by Rosa Biotech (South West Biosciences Doctoral Training Partnership). F.P. was supported by an Engineering and Physical Sciences Research Council (EPSRC) program grant to G.J.G. and D.N.W. (EP/T012455/1). O.A.H., J.F.J., and T.A.A.O. acknowledge financial support from EPSRC for the award of Programme Grant EP/V026690/1. T.A.A.O. acknowledges support from the Royal Society for a University Research Fellowship (UF1402310, URF\R\201007) and Research Fellows Enhancement Award (RF\ERE\210045). The authors thank the Mass Spectrometry Facility, School of Chemistry, University of Bristol, for access to the EPSRC-funded Bruker Ultraflex MALDI−TOF instrument (EP/K03927X/1). The authors would like to thank Diamond Light Source for access to beamline I04 (proposals mx23269 and mx31440). The authors thank internship students at Rosa Biotech, Josh Lewin and Dr Nokomis Ramos-Gonzalez, who conducted ligand docking and molecular dynamics simulations of multiple dyes in αHB, which led to the current work. Finally, the authors thank the members of the Woolfson and Oliver laboratories for many helpful discussions.

■ ABBREVIATIONS

αHB	α-helical barrel
CD	circular dichroism
DPH	1,6-diphenyl-1,3,5-hexatriene
FRET	Förster resonance energy transfer
MD	molecular dynamics
TA	transient absorption
TCSPC	time-correlated single photon counting

■ REFERENCES

(1) Woolfson, D. N. A Brief History of De Novo Protein Design: Minimal, Rational, and Computational. *J. Mol. Biol.* **2021**, *433* (20), 167160.
(2) Dawson, W. M.; Rhys, G. G.; Woolfson, D. N. Towards functional de novo designed proteins. *Curr. Opin. Chem. Biol.* **2019**, *52*, 102−111.
(3) Korendovych, I. V.; DeGrado, W. F. De novo protein design, a retrospective. *Q. Rev. Biophys.* **2020**, *53*, No. e3.
(4) Pan, X.; Kortemme, T. Recent advances in de novo protein design: Principles, methods, and applications. *J. Biol. Chem.* **2021**, *296*, 100558.
(5) Khakzad, H.; Igashov, I.; Schneuing, A.; Goverde, C.; Bronstein, M.; Correia, B. A new age in protein design empowered by deep learning. *Cell Syst.* **2023**, *14* (11), 925−939.
(6) Lovelock, S. L.; Crawshaw, R.; Basler, S.; Levy, C.; Baker, D.; Hilvert, D.; Green, A. P. The road to fully programmable protein catalysis. *Nature* **2022**, *606* (7912), 49−58.
(7) Lu, L.; Gou, X.; Tan, S. K.; Mann, S. I.; Yang, H.; Zhong, X.; Gazgalis, D.; Valdiviezo, J.; Jo, H.; Wu, Y. De novo design of drug-binding proteins with predictable binding energy and specificity. *Science* **2024**, *384* (6691), 106−112.
(8) Polizzi, N. F.; DeGrado, W. F. A defined structural unit enables de novo design of small-molecule−binding proteins. *Science* **2020**, *369* (6508), 1227−1233.
(9) Studer, S.; Hansen, D. A.; Pianowski, Z. L.; Mittl, P. R. E.; Debon, A.; Guffy, S. L.; Der, B. S.; Kuhlman, B.; Hilvert, D. Evolution of a highly active and enantiospecific metalloenzyme from short peptides. *Science* **2018**, *362* (6420), 1285−1288.
(10) Handel, T.; DeGrado, W. F. De novo design of a Zn2+-binding protein. *J. Am. Chem. Soc.* **1990**, *112* (18), 6710−6711.
(11) Korendovych, I. V.; DeGrado, W. F. Catalytic efficiency of designed catalytic proteins. *Curr. Opin. Struct. Biol.* **2014**, *27*, 113−121.
(12) Song, Q.; Cheng, Z.; Kariuki, M.; Hall, S. C. L.; Hill, S. K.; Rho, J. Y.; Perrier, S. Molecular Self-Assembly and Supramolecular Chemistry of Cyclic Peptides. *Chem. Rev.* **2021**, *121* (22), 13936−13995.
(13) Burton, A. J.; Thomson, A. R.; Dawson, W. M.; Brady, R. L.; Woolfson, D. N. Installing hydrolytic activity into a completely de novo protein framework. *Nat. Chem.* **2016**, *8* (9), 837−844.
(14) Lombardi, A.; Pirro, F.; Maglio, O.; Chino, M.; DeGrado, W. F. De Novo Design of Four-Helix Bundle Metalloproteins: One Scaffold, Diverse Reactivities. *Acc. Chem. Res.* **2019**, *52* (5), 1148−1159.
(15) Pirro, F.; La Gatta, S.; Arrigoni, F.; Famulari, A.; Maglio, O.; Del Vecchio, P.; Chiesa, M.; De Gioia, L.; Bertini, L.; Chino, M. A De Novo-Designed Type 3 Copper Protein Tunes Catechol Substrate Recognition and Reactivity. *Angew. Chem., Int. Ed.* **2023**, *62* (1), No. e202211552.
(16) Nastri, F.; D'Alonzo, D.; Leone, L.; Zambrano, G.; Pavone, V.; Lombardi, A. Engineering Metalloprotein Functions in Designed and Native Scaffolds. *Trends Biochem. Sci.* **2019**, *44* (12), 1022−1040.
(17) Song, Q.; Cheng, Z.; Perrier, S. Supramolecular peptide nanotubes as artificial enzymes for catalysing ester hydrolysis. *Polym. Chem.* **2023**, *14* (41), 4712−4718.
(18) Huang, P.-S.; Boyken, S. E.; Baker, D. The coming of age of de novo protein design. *Nature* **2016**, *537* (7620), 320−327.
(19) Lassila, J. K.; Privett, H. K.; Allen, B. D.; Mayo, S. L. Combinatorial methods for small-molecule placement in computational enzyme design. *Proc. Natl. Acad. Sci. U. S. A.* **2006**, *103* (45), 16710−16715.
(20) Röthlisberger, D.; Khersonsky, O.; Wollacott, A. M.; Jiang, L.; DeChancie, J.; Betker, J.; Gallaher, J. L.; Althoff, E. A.; Zanghellini, A.; Dym, O. Kemp elimination catalysts by computational enzyme design. *Nature* **2008**, *453* (7192), 190−195.
(21) Jiang, L.; Althoff, E. A.; Clemente, F. R.; Doyle, L.; Röthlisberger, D.; Zanghellini, A.; Gallaher, J. L.; Betker, J. L.; Tanaka, F.; Barbas, C. F. De Novo Computational Design of Retro-Aldol Enzymes. *Science* **2008**, *319* (5868), 1387−1391.

(22) Ashworth, J.; Havranek, J. J.; Duarte, C. M.; Sussman, D.; Monnat, R. J.; Stoddard, B. L.; Baker, D. Computational redesign of endonuclease DNA binding and cleavage specificity. *Nature* **2006**, *441* (7093), 656−659.
(23) Krishna, R.; Wang, J.; Ahern, W.; Sturmfels, P.; Venkatesh, P.; Kalvet, I.; Lee, G. R.; Morey-Burrows, F. S.; Anishchenko, I.; Humphreys, I. R. Generalized biomolecular modeling and design with RoseTTAFold All-Atom. *Science* **2024**, *384* (6693), No. eadl2528.
(24) Watson, J. L.; Juergens, D.; Bennett, N. R.; Trippe, B. L.; Yim, J.; Eisenach, H. E.; Ahern, W.; Borst, A. J.; Ragotte, R. J.; Milles, L. F. De novo design of protein structure and function with RFdiffusion. *Nature* **2023**, *620* (7976), 1089−1100.
(25) Kortemme, T. De novo protein design—From new structures to programmable functions. *Cell* **2024**, *187* (3), 526−544.
(26) Polizzi, N. F.; Wu, Y.; Lemmin, T.; Maxwell, A. M.; Zhang, S.-Q.; Rawson, J.; Beratan, D. N.; Therien, M. J.; DeGrado, W. F. De novo design of a hyperstable non-natural protein−ligand complex with sub-Å accuracy. *Nat. Chem.* **2017**, *9* (12), 1157−1164.
(27) Hutchins, G. H.; Noble, C. E. M.; Bunzel, H. A.; Williams, C.; Dubiel, P.; Yadav, S. K. N.; Molinaro, P. M.; Barringer, R.; Blackburn, H.; Hardy, B. J. An expandable, modular de novo protein platform for precision redox engineering. *Proc. Natl. Acad. Sci. U. S. A.* **2023**, *120* (31), No. e2306046120.
(28) Siegel, J. B.; Zanghellini, A.; Lovick, H. M.; Kiss, G.; Lambert, A. R.; St Clair, J. L.; Gallaher, J. L.; Hilvert, D.; Gelb, M. H.; Stoddard, B. L. Computational design of an enzyme catalyst for a stereoselective bimolecular Diels-Alder reaction. *Science* **2010**, *329* (5989), 309−313.
(29) Lechner, H.; Oberdorfer, G. Derivatives of Natural Organocatalytic Cofactors and Artificial Organocatalytic Cofactors as Catalysts in Enzymes. *ChemBiochem* **2022**, *23* (13), No. e202100599.
(30) Byrne, M. J.; Lees, N. R.; Han, L.-C.; van der Kamp, M. W.; Mulholland, A. J.; Stach, J. E. M.; Willis, C. L.; Race, P. R. The Catalytic Mechanism of a Natural Diels−Alderase Revealed in Molecular Detail. *J. Am. Chem. Soc.* **2016**, *138* (19), 6095−6098.
(31) Kondo, K.; Klosterman, J. K.; Yoshizawa, M. Aromatic Micelles as a New Class of Aqueous Molecular Flasks. *Chemistry* **2017**, *23* (66), 16710−16721.
(32) Yoshizawa, M.; Klosterman, J. K.; Fujita, M. Functional Molecular Flasks: New Properties and Reactions within Discrete, Self-Assembled Hosts. *Angew. Chem., Int. Ed.* **2009**, *48* (19), 3418−3438.
(33) Fang, Y.; Powell, J. A.; Li, E.; Wang, Q.; Perry, Z.; Kirchon, A.; Yang, X.; Xiao, Z.; Zhu, C.; Zhang, L. Catalytic reactions within the cavity of coordination cages. *Chem. Soc. Rev.* **2019**, *48* (17), 4707−4730.
(34) Gee, W. J. The growing importance of crystalline molecular flasks and the crystalline sponge method. *Dalton Trans.* **2017**, *46* (46), 15979−15986.
(35) Inokuma, Y.; Kawano, M.; Fujita, M. Crystalline molecular flasks. *Nat. Chem.* **2011**, *3* (5), 349−358.
(36) Dawson, W. M.; Martin, F. J. O.; Rhys, G. G.; Shelley, K. L.; Brady, R. L.; Woolfson, D. N. Coiled coils 9-to-5: Rational de novo design of α-helical barrels with tunable oligomeric states. *Chem. Sci.* **2021**, *12* (20), 6923−6928.
(37) Thomas, F.; Dawson, W. M.; Lang, E. J. M.; Burton, A. J.; Bartlett, G. J.; Rhys, G. G.; Mulholland, A. J.; Woolfson, D. N. De Novo-Designed α-Helical Barrels as Receptors for Small Molecules. *ACS Synth. Biol.* **2018**, *7* (7), 1808−1816.
(38) Thomson, A. R.; Wood, C. W.; Burton, A. J.; Bartlett, G. J.; Sessions, R. B.; Brady, R. L.; Woolfson, D. N. Computational design of water-soluble alpha-helical barrels. *Science* **2014**, *346* (6208), 485−488.
(39) Hagiwara, K.; Akita, M.; Yoshizawa, M. An aqueous molecular tube with polyaromatic frameworks capable of binding fluorescent dyes. *Chem. Sci.* **2015**, *6* (1), 259−263.
(40) Xu, C.; Liu, R.; Mehta, A. K.; Guerrero-Ferreira, R. C.; Wright, E. R.; Dunin-Horkawicz, S.; Morris, K.; Serpell, L. C.; Zuo, X.; Wall, J. S. Rational Design of Helical Nanotubes from Self-Assembly of Coiled-Coil Lock Washers. *J. Am. Chem. Soc.* **2013**, *135* (41), 15565−15578.
(41) Dawson, W. M.; Shelley, K. L.; Fletcher, J. M.; Scott, D. A.; Lombardi, L.; Rhys, G. G.; Lagambina, T. J.; Obst, U.; Burton, A. J.; Cross, J. A. Differential sensing with arrays of de novo designed peptide assemblies. *Nat. Commun.* **2023**, *14*, 1.
(42) Jain, B.; Das, K. Fluorescence resonance energy transfer between DPH and Nile Red in a lipid bilayer. *Chem. Phys. Lett.* **2006**, *433* (1), 170−174.
(43) Eberhardt, J.; Santos-Martins, D.; Tillack, A. F.; Forli, S. AutoDock Vina 1.2.0: New Docking Methods, Expanded Force Field, and Python Bindings. *J. Chem. Inf. Model.* **2021**, *61* (8), 3891−3898.
(44) Cehelnik, E. D.; Cundall, R. B.; Lockwood, J. R.; Palmer, T. F. Solvent and temperature effects on the fluorescence of all-trans-1,6-diphenyl-1,3,5-hexatriene. *J. Phys. Chem.* **1975**, *79* (14), 1369−1376.
(45) Ray, A.; Das, S.; Chattopadhyay, N. Aggregation of Nile Red in Water: Prevention through Encapsulation in β-Cyclodextrin. *ACS Omega* **2019**, *4* (1), 15−24.
(46) Ghoneim, N. Photophysics of Nile red in solution: Steady state spectroscopy. *Spectrochim. Acta, Part A* **2000**, *56* (5), 1003−1010.
(47) Gajo, C.; Shchepanovska, D.; Jones, J. F.; Karras, G.; Malakar, P.; Greetham, G. M.; Hawkins, O. A.; Jordan, C. J. C.; Curchod, B. F. E.; Oliver, T. A. A. Nile Red Fluorescence: Where's the Twist? *J. Phys. Chem. B* **2024**, *128* (47), 11768−11775.
(48) Tamaki, T.; Kokubu, T. Acceleration of the photodimerization of water-soluble anthracenes included by β- and γ-cyclodextrins. *J. Inclusion Phenom.* **1984**, *2* (3), 815−822.
(49) Albanese, K. I.; Petrenas, R.; Pirro, F.; Naudin, E. A.; Borucu, U.; Dawson, W. M.; Scott, D. A.; Leggett, G. J.; Weiner, O. D.; Oliver, T. A. A.; et al. Rationally seeded computational protein design of α-helical barrels. *Nat. Chem. Biol.* **2024**, *20*, 991.
(50) Bunzel, H. A.; Anderson, J. L. R.; Mulholland, A. J. Designing better enzymes: Insights from directed evolution. *Curr. Opin. Struct. Biol.* **2021**, *67*, 212−218.

https://doi.org/10.1021/jacs.4c16633
J. Am. Chem. Soc. 2025, 147, 3796−3803